Int. J. Electrochem. Sci., 7 **(2012)** 4585 - 4595

International Journal of
ELECTROCHEMICAL
SCIENCE
www.electrochemsci.org

Processing and Evaluation of Alumina Doped Nickel Ferrite Nano-Particles

N. M. Deraz[1,2,*] *and A. Alarifi*[1]

[1] Catalytic chemistry chair, Chemistry Department, College of Science, Riyadh, King Saud University, Saudi Arabia
[2]Physical Chemistry Department, Laboratory of Surface Chemistry and Catalysis, National Research Center, Dokki, Cairo, Egypt
[*]E-mail: nmderaz@yahoo.com

Received: 12 March 2012 / *Accepted:* 27 March 2012 / *Published:* 1 May 2012

Alumina doped nickel ferrite nano-particles have been synthesized by the combustion route. Characterization of the products carried out using X-ray diffraction (XRD) and scanning electron microscopy (SEM). Magnetic and surface properties of the as prepared ferrites were determining by using vibrating sample magnetometer (VSM) and N_2 adsorption at 77 K. X-ray analysis showed that all samples consisted of cubic spinel nickel ferrite. The increase in alumina content brought about a decrease in all lattice parameters of Ni ferrite. The combustion method led to formation of spongy and fragile network structure. Increasing amounts of alumina brought about remarkable changes in the microstructure and porosity of nickel ferrite. Alumina doping resulted in an increase in the surface area of Ni ferrite. This treatment led to a decrease in saturation magnetization of the synthesized ferrite.

Keywords: XRD; SEM; VSM; $NiFe_2O_4$; S_{BET}; alumina doping

1. INTRODUCTION

Transition metal ferrites have a primary position of economic and engineering importance within the family magnetic materials because of their excellent physical properties. Portable radios can be use of a pencil of ferrite as an antenna core. High quality filter coils, transformers of long distance carrier telephone and the fly back transformers of television sets are employing ferrite cores. Different factors affect various physical properties of nano-crystalline ferrites such as distribution of cations among the sub lattices, nature of grain, voids, homogeneity, surface layers, doping, molar ratio, precursors etc. [1–5]. Such factors are preparation method, molar ratio of precursors, history of materials, thermal treatment and doping etc... [5].

Ferrites can be prepared using different methods like: the conventional method that needs high preparation temperatures and long reaction periods, resulting in low surface area ferrites [6]; the coprecipitation method [7] that requires enormous efforts to ensure a homogeneous material with uniform particle size and composition; the sol–gel route that has been promising in obtaining materials with high surface area [8, 9]. But sol–gel method presents the disadvantages of the relative high costs of the metal alkoxides and the release of large amounts of alcohol during the calcination step which requires safety considerations; microwave heating [10] that has been used for the development of a texture that may not be accessible by conventional heating, however is limited by the low tendency of some materials to absorb microwave radiation; and the sonochemical method that uses the ultrasound irradiation during the homogeneous precipitation of the precursor to reduce the effective precipitation time of the precursor [11]. In addition, there are the combustion reaction method that has proved effective in the production of powders with nanometric particle sizes and good crystallinity, and it allows monophases to be obtained in most systems. This method is easy, safe and fast, and allows for the reproduction of ceramic powders on a semi-pilot-scale [12,13]. The combustion flame time and temperature are fundamental factors that affect the final characteristics of powders prepared by the combustion route. The driving force for this route is the released energy which leads to crystallite growth and formation of the desired phase. These factors can be adjusted by varying the synthesis conditions such as the type and amount of fuel [12]. Among the different ferrites, nickel ferrite ($NiFe_2O_4$) has an inverse spinel structure with Ni^{2+} ions in the octahedral (B) sites and Fe^{3+} ions equally distributed between tetrahedral (A) and octahedral (B) sites with formula $(Fe^{3+})_A[Ni^{2+}Fe^{3+}]_BO_4^{2-}$ [12].

The doping with various metal cations allows some tunable changes in the different properties of various ferrites [14-16]. Several authors had studied the effects of the doping by zinc, niobium and magnesium on the different properties of nickel ferrite [17-19]. Nanocrystalline Zn- doped nickel ferrite had synthesized from a stoichiometric mixture of corresponding metal nitrates and urea. Magnetic properties of this ferrite showed anomalities as the Zn doping level increased. This has been explained and attributed to the relative positions of Ni, Zn, and Fe ions in the crystal lattice [17]. Some researchers studied the effect of niobium-doping on the structural, electrical and magnetic properties of nickel ferrite. They found that doping of nickel ferrite with niobium ion led to decrease in both their size and magnetization with an increase in the coercive field. This behavior can be explained introducing core-shell model of magnetic nano-particles [18, 19]. Deraz reported that nano-crystalline magnesia doped nickel ferrite powders have been synthesized by the combustion route. The doping of nickel ferrite with magnesia resulted in a decrease in the average crystallite size, lattice constant, unit cell volume, X-ray density, ionic radii, the distance between the magnetic ions and bond lengths on tetrahedral sites and octahedral sites of the as prepared ferrite. In addition, this treatment led to a decrease in its saturation magnetization of nickel ferrite [20].

The present work is focused on the effects of alumina-doping on the structural, morphological and magnetic properties of nickel ferrite obtained via combustion route. The X-ray powder diffraction patterns, the microstructure and the magnetic properties are discussed as a function of the dopant content. The techniques employed were XRD, SEM, N_2 adsorption and VSM.

2. EXPERIMENTAL

2.1. Preparation route

Alumina doped nickel ferrite samples were prepared by mixing calculated proportions of nickel and iron nitrates with urea in presence of different amounts of aluminum nitrate. The mixed precursors were concentrated in a porcelain crucible on a hot plate at 350 ^{o}C for 5 minutes. The crystal water was gradually vaporized during heating and when a crucible temperature was reached, a great deal of foams produced and spark appeared at one corner which spread through the mass, yielding a voluminous and fluffy product in the container. The as-synthesized products were heat treated at 700 ^{o}C for 1 h to enhance their crystallinity and remove the residual charred organic materials. In this investigation, the concentrations of alumina expressed as wt % Al_2O_3 were 0.5, 1.0 and 1.5. The chemicals employed in the present work were of analytical grade supplied by Prolabo Company.

2.2. Characterization techniques

An X-ray measurement of various mixed solids was carried out using a BRUKER D8 advance diffractometer (Germany). The patterns were run with Cu K_α radiation at 40 kV and 40 mA with scanning speed in 2θ of 2 ° min^{-1}.

The crystallite size of undoped and Al_2O_3-doped $NiFe_2O_4$ present in the investigated solids was based on X-ray diffraction line broadening and calculated by using Scherrer equation [21].

$$d = \frac{B\lambda}{\beta \cos\theta} \qquad (1)$$

where d is the average crystallite size of the phase under investigation, B is the Scherrer constant (0.89), λ is the wave length of X-ray beam used, β is the full-width half maximum (FWHM) of diffraction and θ is the Bragg's angle.

Scanning electron micrographs (SEM) was recorded on JEOL JAX-840A electron microanalyzer. The samples were dispersed in ethanol and then treated ultrasonically in order to disperse individual particles over gold grids.

2.3. Surface properties

The surface features of various nano-crystalline catalysts, namely, The specific surface area (S_{BET}), total pore volume (V_p) and mean pore radius (ŕ) were estimated from nitrogen adsorption isotherms measured at 77 K, using Nova 2000, Quanta Chrome (commercial BET unit). Before undertaking such measurements, each sample was degassed under a reduced pressure of 10^{-5} Torr for 2 h at 200 ^{o}C.

2.4. Magnetic properties

The magnetic properties of the investigated solids were measured at room temperature using a vibrating sample magnetometer (VSM; 9600-1 LDJ, USA) in a maximum applied field of 15 kOe. From the obtained hysteresis loops, the saturation magnetization (M_s), remanence magnetization (M_r) and coercivity (H_c) were determined.

3. RESULTS

3.1. XRD analysis

An X-ray diffraction pattern of undoped and alumina doped nickel ferrite nano-particles were determined in Fig.1.

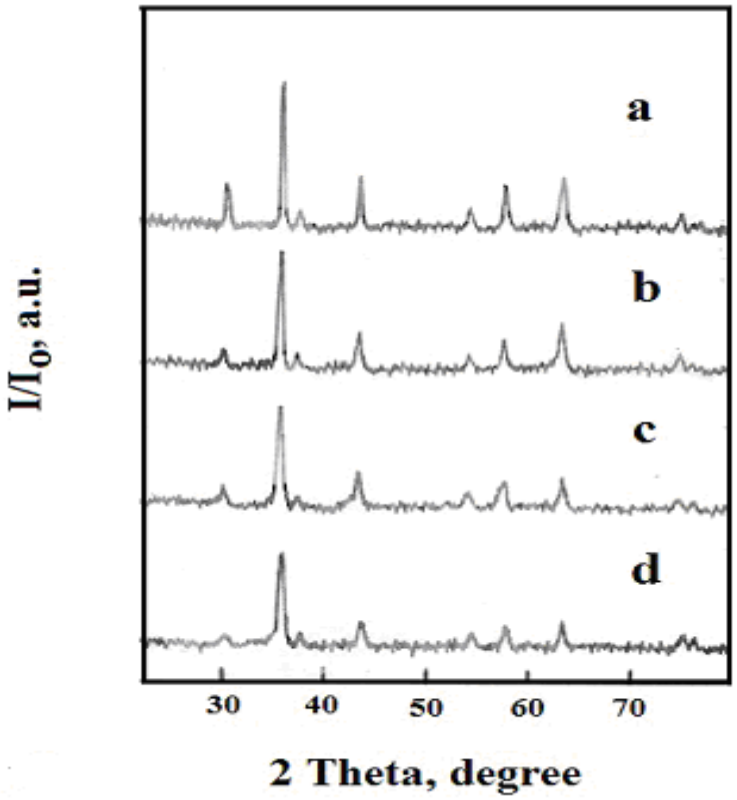

Figure 1. XRD patterns for undoped and Al- doped nickel ferrite samples: (a) 0.00; (b) 0.5; (c) 1.0 and (d) 1.5 wt % Al_2O_3.

This figure displays formation of well nano-crystalline undoped and alumina doped $NiFe_2O_4$ solids as a single cubic spinel phase with reflection planes (2 2 0), (3 1 1), (4 0 0), (4 2 2), (5 1 1), (4 4 0), (6 2 0) and (5 3 3). An increase of the alumina content resulted in a measurable decrease in the

degree of crystallinity of spinel nickel ferrite phase with subsequent a decrease in the intensity of its diffraction peaks.

Some diffraction planes such as (2 2 0) and (4 4 0) planes are more sensitive to the cations distribution on tetrahedral and octahedral sites, respectively [1, 16].

Table 1. The effects of alumina doping on the intensity values of hkl planes of $NiFe_2O_4$ phase.

Concentration of Al_2O_3 (wt%)	Peak height (a. u.)	
	I_{220}	I_{440}
0.0	27	45
0.5	24	40
1.0	22	33
1.5	20	23

Table 1 shows the intensities of the previous two planes. It can be observed that the intensities of these planes decrease with the addition of alumina indicating to the preference of the Al^{3+} by the octahedral and tetrahedral sites. Indeed, The decrease in the intensity of the (2 2 0) plane is smaller than that of the (4 4 0) plane. This result might show the increasing amounts of Al^{3+} located on octahedral sites due to Al- doping process. From literature, Al^{3+} ions have strong preference for the octahedral sites. On the basis of this data and on earlier studies [22], the inverse spinel structure can be assigned in the synthesized materials having the formula $NiAl_xFe_{2-x}O_4$ and can be expressed as:

$$(Fe_{1-\delta}^{3+}\ Al_{\delta})_A[Ni^{2+}Al_{x-\delta}^{3+}\ Fe_{1-x-\delta}^{3+}]_B\ O_4^{2-} \qquad (2)$$

where x and δ are concentrations of Al^{3+} ions in different sites.

The structural parameters of undoped and alumina doped nickel ferrite such as the crystallite size (d), lattice constant (a), unit cell volume (V), X-ray density (D_x), ionic radii (r_A and r_B), the distance between the magnetic ions (L_A and L_B) and bond lengths (A–O and B–O) on tetrahedral (A) sites and octahedral (B) sites of cubic spinel structure can be determined from the data of X-ray. The estimated values of various structural parameters are given in Tables 2 and 3.

Table 2. The effects of alumina doping on some structural parameters of nickel ferrite.

Concentration of Al_2O_3 (wt%)	d (nm)	a (nm)	V (nm^{-3})	D_x (g/cm^3)
0.0	60	0.8338	0.5797	5.582
0.5	45	0.8322	0.5763	5.615
1.0	38	0.8318	0.5755	5.623
1.5	30	0.8308	0.5734	5.643

Table 3. The effects of alumina doping on the values of L_A, L_B, A-O, B-O, r_A and r_B of nickel ferrite.

Concentration of Al_2O_3 (wt%)	L_A (nm)	L_B (nm)	A-O (nm)	B-O (nm)	r_A (nm)	r_B (nm)
0.0	0.3610	0.2948	0.2021	0.1959	0.0671	0.0609
0.5	0.3603	0.2942	0.2018	0.1956	0.0669	0.0606
1.0	0.3602	0.2941	0.2016	0.1955	0.0666	0.0605
1.5	0.3597	0.2937	0.2014	0.1952	0.0662	0.0602

It can be seen from Table 2 that the rise in the concentration of aluminum species brought about a decrease in the values of crystallite size, lattice constant and unit cell volume of the as synthesized ferrite. Opposite behavior was observed for the value of X-ray density. However, the results in Table 3 showed that the values of L_A, L_B, r_A, r_B, A–O and B–O decrease as the amount of Al species increases. These findings could be attributed to the incorporation of aluminum ions, having smaller ionic radii, in the lattice of nickel ferrite with subsequent redistribution of cations among octahedral and tetrahedral sites [22]. In the present series $NiAl_xFe_{2-x}O_4$, larger Fe^{3+} (0.067 nm) ions are replaced by smaller Al^{3+} (0.051 nm) ions; therefore, the decrease in lattice constant takes place [22].

3.2. Surface properties

The various surface characteristics, namely, S_{BET}, V_p and ŕ of various solids were determined from N_2 adsorption isotherms conducted 77K. The different surface parameters of various investigated solids are given in Table 4. The data in this table showed that the values of $S_{BET}$for the synthesized nickel ferrite decreased by increasing the dopant content. Opposite behavior was observed for the values of V_p and ŕ.

Table 4. The effects of alumina doping on the surface properties of the as prepared solids.

Concentration of Al_2O_3 (wt%)	S_{BET} (m^2/g)	V_p (cc/g)	r' (nm)
0.0	19	0.0504	5.3
0.5	25	0.0401	3.2
1.0	29	0.0330	2.3
1.5	36	0.0180	1.1

This increase in the surface area due to alumina doping could be attributed to a pore-narrowing process depending upon decrease of both the total pore volume and the mean pore radius of the tested solids. It was reported that S_{BET} of the undoped sample measures about 19 m^2 g^{-1} and increases to 36 m^2 g^{-1} for the sample doped with 1.5 wt % Al_2O_3. In other words, the maximum increase in the S_{BET} of

Ni ferrite due to the doping with 1.5 wt% Al_2O_3 attained 89.5%. Also, the maximum decrease in both total pore volume and mean pore radius is 64.3 and 81 % for the sample doped with 1.5 wt % Al_2O_3, respectively. One can not overlook the decrease in the crystallite size which leads to an increase in surface area of the as prepared solids.

3.3. SEM analysis

The morphological characteristics of the pure and nickel ferrite doped with 0.5 and 1.5 wt% Al_2O_3 were determined by SEM.

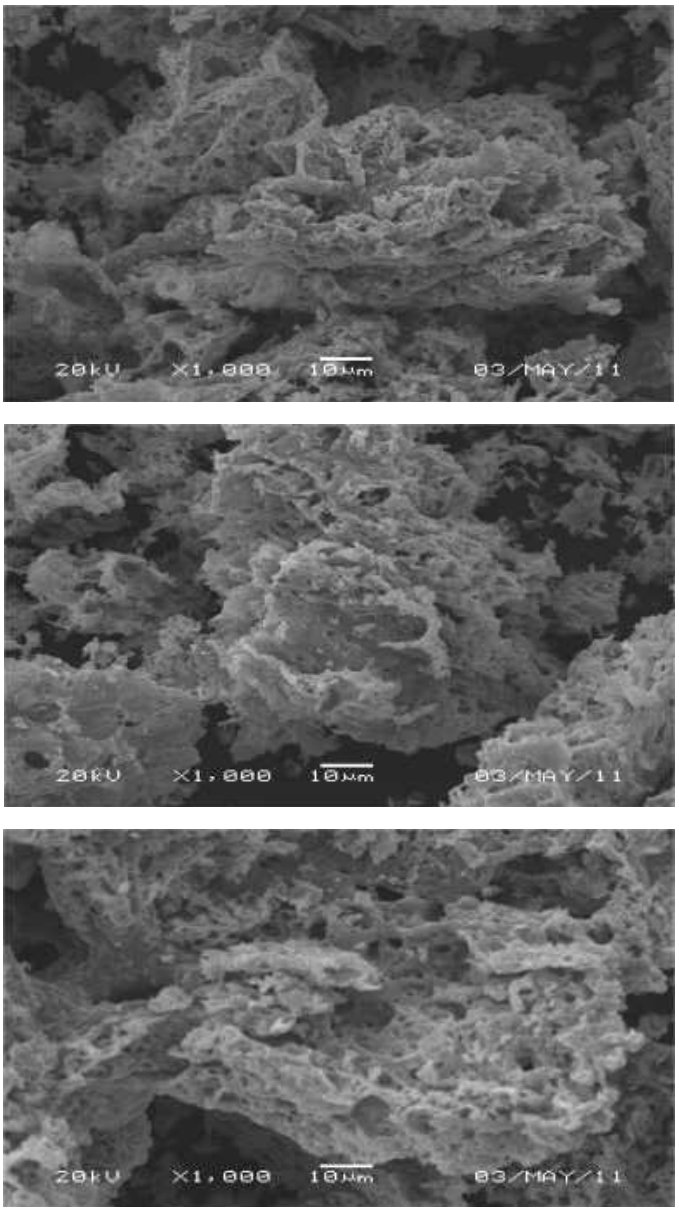

Figure 2. SEM images for undoped and Al- doped nickel ferrite samples: (a) 0.00; (b) 0.5 and (c) 1.5 wt % Al_2O_3.

SEM images are given in Fig. 2a-c of undoped and doped nickel ferrite samples reveal remarkable changes in the microstructure. One can see the formation of spongy and fragile network structure. The voids and pores present in the samples are attributed to the release of some gases during combustion process. The increase in the amount of alumina brought about a decrease in the extent of voids and pores with week agglomeration of the powders. This confirmed by the textural measurements of the as prepared ferrite. Indeed, the increase in the amount of alumina led to a decrease in the total pore volume of nickel ferrite. This indicates to a decrease of porosity of nickel ferrite by alumina doping.

3.4. Magnetic properties

Magnetic hysteresis loops observed for the undoped and Al- doped nickel ferrite system at room temperature and applied field of 15 kG are shown in Fig. 3.

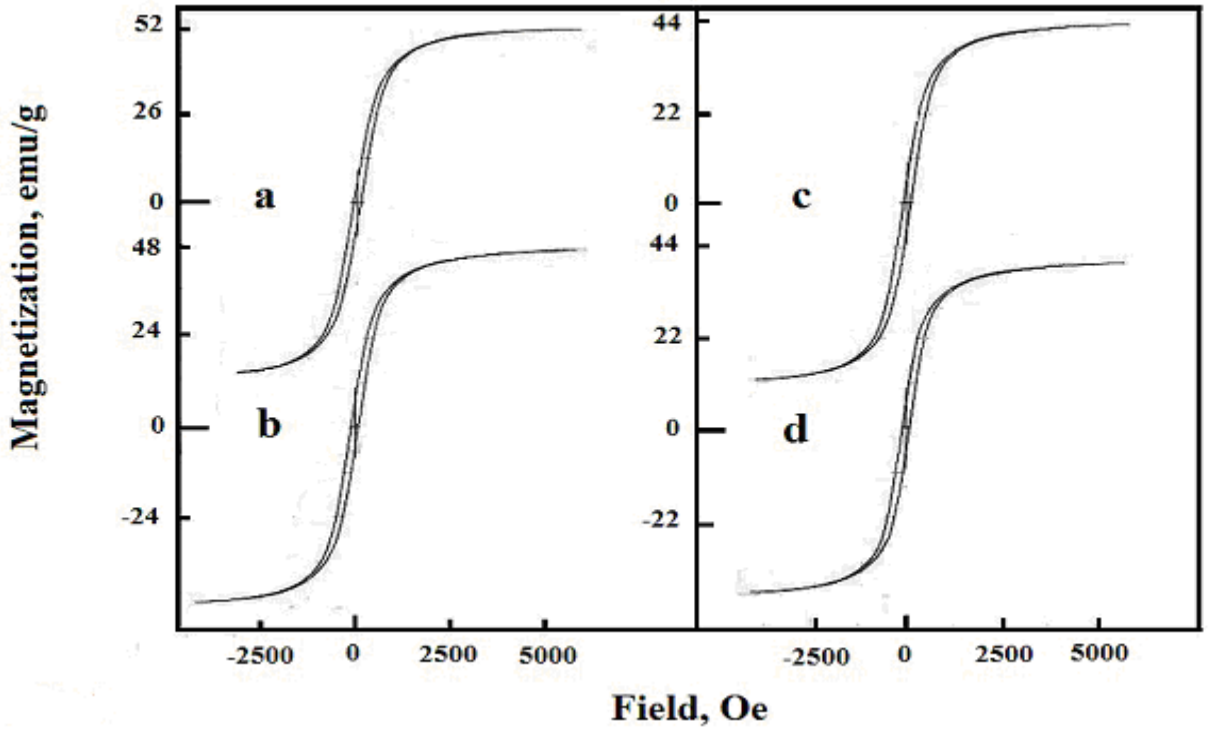

Figure 3. Magnetic hysteresis curves measured at a room temperature for undoped and Al- doped nickel ferrite samples: (a) 0.00; (b) 0.5; (c) 1.0 and (d) 1.5 wt % Al_2O_3.

The effects of the doping with alumina on the values of the saturation magnetization (M_s), remanence magnetization (M_r) and coercivity (H_c) and magnetic moment (n_B) of the nickel ferrite are tabulated in Table 5. Investigation of Table 5 reveals that: (i) the increase in the amount of alumina led to a decrease in the values of saturation magnetization and remanence magnetization of nickel ferrite.

Table 5. The effects of alumina doping on the magnetic properties (M_s, M_r and H_c) of the as-prepared solids.

Concentration of Al_2O_3 (wt %)	M_s (emu/g)	M_r (emu/g)	M_r/M_s (emu/g)	H_c (Oe)	n_B
0.0	52	13.98	0.269	92.46	2.184
0.5	47	13.81	0.293	98.64	1.974
1.0	44	13.07	0.297	97.36	1.848
1.5	40	12.85	0.321	100. 10	1.680

The maximum decrease in the value of M_s and M_r of Ni ferrite due to the doping with 1.5 wt% Al_2O_3 attained 23.1and 8.1%, respectively. (ii) The value of magnetic moment (n_B) decreases as the concentration of Al species in doped nickel ferrite increases. The maximum decrease in the value of n_B due to 1.5 wt% Al_2O_3- doping attained 23.1%. (iii) The treatment of nickel ferrite with different amounts of alumina brought about slightly increase in the value of H_c. The dissolution of Al^{3+} ions in the lattices of NiO and Fe_2O_3, involved in the forming nickel ferrite, can proceed via substitution of some host Ni^{2+} and Fe^{3+} ions and/or also by their location in interstitial positions forming solid solution. This dissolution led to re-orientation and contraction of the cations included in the nickel ferrite formation. These findings brought about significant changes in the magnetic properties.

4. DISCUSSION

Systematic doping of some spinel ferrite (especially prepared by combustion route) with different elements and the underlying study of structural, morphemically; magnetic properties are not extensively documented. The combustion technique yields nanocrystalline single-phase ferrites. The XRD pattern shows the formation of single-phase cubic spinel structure for all the samples. The diffraction peaks of the as prepared solids are broader with the increase in the aluminum content, which may be due to distribution of nanocrystallities. The decrease in the lattice constant of nickel ferrite due to the increase in the aluminum content could be attributed to the difference in ionic radii of Fe^{3+} and Al^{3+} ions.

The dissolution of Al^{3+} ions in the lattices of NiO and Fe_2O_3, involved in the forming nickel ferrite, can proceed via substitution of some host Ni^{2+} and Fe^{3+} ions and/or also by their location in interstitial positions forming solid solution. The dissolution process can be simplified by the use of Kröger's notations [23] in the following manner:

$$Al_2O_3 \rightarrow 2Al(Ni^{2+}) + C.V \quad (3)$$

$$Al_2O_3 \rightarrow Al(Fe^{3+}) + C.V \quad (4)$$

$$Al_2O_3 + 2Ni^{2+} \rightarrow 2Al_{\Delta} + 2\,Ni^{2+} + C.V \quad (5)$$

$$Al_2O_3 + 2Fe^{3+} \rightarrow 2Al_{\Delta} + 2Fe^{3+} + 2C.V \quad (6)$$

$Al(Ni^{2+})$ and $Al(Fe^{3+})$ are the trivalent aluminium ions located in the positions of host nickel and iron oxides in NiO and Fe_2O_3, respectively; Al_{Δ} is aluminium ions located in the interstitial positions of nickel and ferric oxide lattices; C.V. created cationic vacancies. The dissolution of dopant ions in the lattices of reacting oxides according to the previous reactions (3, 4, 5 and 6) which led to creation of cationic vacancies might increase the mobility of cations of reacting oxides (Ni^{2+} and Fe^{3+}) with subsequent an increase in the ferrite formation.

Measured magnetic properties including the room temperature magnetic hysteresis loops of our samples show reduction of both saturation magnetization and remanent magnetization with the increase in the aluminum content. The largest saturation magnetization was 52 emu/g for undoped sample, which is near to the multi-domain bulk nickel ferrite (55 emu/g) [24]. The reduction in the saturation magnetization comes from the non-collinearity induced by finite size and surface effects [25-27]. In fact, alumina doping of nickel ferrite resulted in an increase in the surface area with subsequent decrease in the crystallite size. Consequently, the saturation magnetization of nickel ferrite decreases for smaller sizes [27-29]. However, the decrease of saturation magnetization and remanent magnetization with the increase in the aluminum content occurs because the replacement of Fe^{3+} by Al^{3+} ions weaken the sub lattice interaction and lowers the magnetic moment of unit cells. The magnetic moment of nickel ferrite decreases from 2.184 to 1.68 by doping with1.5 wt% Al_2O_3.

5. CONCLUSIONS

Nano-crystalline undoped and alumina doped nickel ferrite can be prepared by the combustion method. The structural, morphology and magnetic properties of the obtained materials have been studied. The formation of single cubic phase $NiFe_2O_4$ was confirmed by the XRD technique. SEM measurements showed the homogeneity of the as prepared solids. The lattice constant, unit cell volume, ionic radii, the distance between the magnetic ions and bond lengths on tetrahedral sites and octahedral sites of cubic spinel structure were found to decrease with the increase in alumina concentration. The average crystallite size decreases as the concentration of Al species increases. Alumina doping of nickel ferrite brought about a decrease in both total pore volume and mean pore radius with subsequent increase in the surface area. The saturation magnetization was found to decrease with the increase in alumina content.

ACKNOWLEDGEMENT
This work was supported by NPST program by King Saud University Project: Number 09-ADV651-02.

References

1. K. M. Batoo, S. Kumar, R. Prakash, Alimuddin, I. Song, H. Chung, H. Jeong, C.G. Lee, *J. Cent. South Univ. Technol.* 17 (2010) 1129.
2. S. Kumar, A.M.M. Farea, K.M. Batoo, C.G. Lee, B.H. Koo, A. Yousef, Alimuddin, *Physica B* 403 (2008)3604.
3. K. M. Batoo, S.Kumar,C.G.Lee, Alimuddin, *J.Alloy Compds* 480(2009)596.
4. Mohd. Hashim, Alimuddin, Shalendra Kumar, Sikander Ali, B. H. Koo, H. Chung, Ravi Kumar, *J.Alloy Compds* 511(2012)107.
5. N. M. Deraz, *J. Anal. Appl. Pyrolysis*, 82(2008) 21.
6. T. Karpova, V. Vassiliev, E. Vladimirova, V. Osotov, M. Ronkin, A. Nosov, *Ceramics International* 38 (2012) 373.
7. M. S. Niasari, F. Davar, T. Mahmoudi, *Polyhedron* 28 (2009) 1455.
8. D. H. Chen, X.R. He, *Mater. Res. Bull*. 36 (2001) 1369.
9. P. Sivakumar, R. Ramesh, A. Ramanand, S. Ponnusamy, C. Muthamizhchelvan, *Mater. Res. Bull*. 46(2011)2208.
10. V. K. Sankaranarayana, C. Sreekumar, *Curr. Appl. Phys*. 3 (2003) 205.
11. L. Wei-zhong, L. Bo, and W. Shao-hui, *Journal of Shenzhen University Science and Engineering* 23(2006)329.
12. A. Alarifi, N. M. Deraz and S. Shaban, *J.Alloy Compds* 486 (2009) 501.
13. N.M. Deraz, S.A. Shaban, A. Alarifi, *J. Saudi Chemical Society* 14(2010)357.
14. E. Rezlescu, N. Rezlescu, P. D. Popa, L. Rezlescu, C. Pasnicu, M. L. Craus, *Mater. Res. Bull*. 33(6)(1998)915.
15. N. M. Deraz, A. Alarifi, *Polyhedron* 28(2009) 4122.
16. N. M. Deraz, *J. Anal. Appl. Pyrolysis* 91(2011) 48.
17. A. C. F. M. Costa, V.J. Silva, D. R. Cornejo, M.R. Morelli, R.H.G.A. Kiminami, L. Gama, *J. Magn. Magn. Mater.* 320 (2008) e370.
18. M. Sertkol, Y. Koseoğlu, A. Baykal, H. Kavas, A. Bozkurt, M.S. Toprak, *J. Alloy Compds* 486 (2009) 325.
19. S. Mishra, N. Karak, T.K. Kundu, D. Das, N. Maity, D. Chakravorty, *Mater. Lett.* 60 (2006) 1111.
20. N. M. Deraz, *Ceramic International* 38 (2012) 511.
21. B.D. Cullity, Elements of X-ray Diffraction, Addison-Wesly Publishing Co. Inc. 1976 (Chapter 14).
22. A.T. Raghavender, Damir Pajic, Kreso Zadro, Tomislav Milekovic, P. Venkateshwar Rao, K.M. Jadhav, D. Ravinder, *J. Magn. Magn. Mater*. 316 (2007) 1.
23. F. A. Kröger, Chemistry of Imperfect Crystals, North-Holland, Amsterdam, 1964.
24. J. Smit, H.P.J. Wijn, Ferrites—Physical Properties of Ferromagnetic Oxides in Relation to their Technical Applications, Wiley, New York, 1959.
25. F. Li, H. Wang, L. Wang, J. Wang, *J. Magn. Magn. Mater*. 309 (2007)295.
26. Y. Koseoğlu, H. Kavas, *J. Nanosci. Nanotechnology* 8 (2008) 584.
27. J.M.D. Coey, *Phys. Rev. Lett*. 27 (1971) 1140.
28. A.E. Berkowitz, J.A. Lahut, I.S. Jacobs, L.M. Levinson, D.W. Forester, *Phys. Rev. Lett*. 34 (1975) 594.
29. A.E. Berkowitz, J.A. Lahut, C.E. VanBuren, , *IEEE Trans on Magn. MAG- 16* (1980) 184.